



Published in final edited form as:

*Cancer Cell*. 2016 May 9; 29(5): 669–683. doi:10.1016/j.ccell.2016.03.027.

## Olig2-Dependent Reciprocal Shift in PDGF and EGF Receptor Signaling Regulates Tumor Phenotype and Mitotic Growth in Malignant Glioma

Fanghui Lu<sup>1,2</sup>, Ying Chen<sup>2,3</sup>, Chuntao Zhao<sup>2</sup>, Haibo Wang<sup>2</sup>, Danyang He<sup>4</sup>, Lingli Xu<sup>2</sup>, Jincheng Wang<sup>2</sup>, Xuelian He<sup>2</sup>, Yaqi Deng<sup>2</sup>, Ellen E. Lu<sup>2</sup>, Xue Liu<sup>3</sup>, Ravinder Verma<sup>2</sup>, Hong Bu<sup>1</sup>, Rachid Drissi<sup>2</sup>, Maryam Fouladi<sup>2</sup>, Anat O Stemmer-Rachamimov<sup>5</sup>, Dennis Burns<sup>4</sup>, Mei Xin<sup>2</sup>, Joshua B. Rubin<sup>6</sup>, El Mustapha Bahassi<sup>7</sup>, Peter Canoll<sup>8</sup>, Eric C Holland<sup>9</sup>, and Q. Richard Lu<sup>2,10,#</sup>

<sup>1</sup>Laboratory of Pathology, State Key Laboratory of Biotherapy, West China Hospital, Sichuan University and National Collaborative Innovation Center, Chengdu, 610041, China

<sup>2</sup>Department of Pediatrics, Brain Tumor Center, Division of Experimental Hematology and Cancer Biology, Cincinnati Children's Hospital Medical Center, Cincinnati, OH 25229, USA

<sup>3</sup>School of Life Sciences, Xiamen University, Fujian, 361102, China

<sup>4</sup>Department of Pathology & Integrative Biology Program, University of Texas Southwestern Medical Center, Dallas, Texas 75390, USA

<sup>5</sup>Department of Pathology, Massachusetts General Hospital, Harvard Medical School, Boston, Massachusetts, USA

<sup>6</sup>Departments of Pediatrics and Anatomy and Neurobiology, Washington University School of Medicine, St Louis, Missouri, USA

<sup>7</sup>Department of Internal Medicine, UC Brain Tumor Center, University of Cincinnati, Cincinnati OH, USA

<sup>8</sup>Department of Pathology & Cellular Biology, Columbia University Medical Center, New York, NY 10032, USA

Correspondence: Q. Richard Lu, Department of Pediatrics, Brain Tumor Center, Division of Experimental Hematology and Cancer Biology, Cincinnati Children's Hospital Medical Center, OH 25229, USA; Tel: 513-636-7684; Fax: 513-803-0783; richard.Lu@cchmc.org.

**Publisher's Disclaimer:** This is a PDF file of an unedited manuscript that has been accepted for publication. As a service to our customers we are providing this early version of the manuscript. The manuscript will undergo copyediting, typesetting, and review of the resulting proof before it is published in its final citable form. Please note that during the production process errors may be discovered which could affect the content, and all legal disclaimers that apply to the journal pertain.

### ACCESSION NUMBERS

All the RNA-seq and ChIP-seq datasets are deposited in the NCBI Gene Expression Omnibus (GEO) GSE71493.

### SUPPLEMENTAL INFORMATION

Supplemental Information includes Supplemental Experimental Procedures and six figures can be found with this article online.

### AUTHOR CONTRIBUTIONS

Q.R.L. and F.L. designed the experiments, analyzed the data and wrote the manuscript with input from all authors. F.L., Y.C., C.Z., H.W., D.H., L.X., J.W., X.H., Y.D., E.E.L., X.L. and R.V. carried out the in vitro, in vivo, gene profiling or in silico analyses. H.B., R.D., M.F., A.O.S., D.B., M.X., J.B.R. E.M.B. provided samples and inputs. P.C. provided PDGF retroviral vectors and data interpretation. E.C.H. provided tumor cell lines and input. Q.R.L. supervised the project.

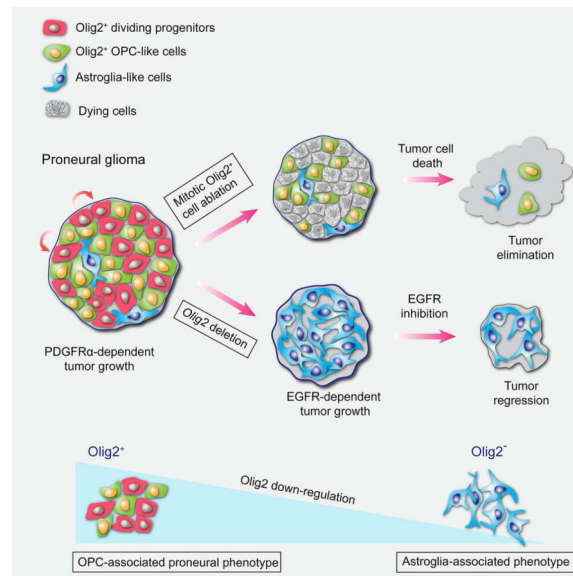
<sup>9</sup>Division of Human Biology and Solid Tumor Translational Research, Fred Hutchinson Cancer Research Center, Alvord Brain Tumor Center, University of Washington, Seattle, WA 98109, USA

<sup>10</sup>Key Laboratory of Birth Defects, Children's Hospital of Fudan University, Shanghai, China, 201102

## Summary

Malignant gliomas exhibit extensive heterogeneity and poor prognosis. Here we identify mitotic Olig2-expressing cells as tumor-propagating cells in proneural gliomas, elimination of which blocks tumor initiation and progression. Intriguingly, deletion of *Olig2* resulted in tumors that grow, albeit at a decelerated rate. Genome occupancy and expression profiling analyses reveal that Olig2 directly activates cell proliferation machinery to promote tumorigenesis. *Olig2* deletion causes a tumor phenotypic shift from an oligodendrocyte precursor-correlated proneural toward astroglia-associated gene expression pattern, manifest in down-regulation of PDGF receptor-alpha and reciprocal up-regulation of EGFR. *Olig2* deletion further sensitizes glioma cells to EGFR inhibitors and extends animal lifespans. Thus, Olig2-orchestrated receptor signaling drives mitotic growth and regulates glioma phenotypic plasticity. Targeting Olig2 may circumvent resistance to EGFR-targeted drugs.

## Graphical Abstract



## Introduction

Glioblastoma (GBM) is the most common malignant brain tumor in adults, exhibiting distinct molecular characteristics, and patients have very poor prognosis with a median survival of less than one year despite aggressive treatments (Jansen et al., 2010). Tumors are resistant to conventional radiotherapy and chemotherapies, and the efficacy of current treatments is limited (Ohgaki and Kleihues, 2005; Schonberg et al., 2014). Based on gene expression profiles, GBMs have been classified into four distinct molecular subtypes,

namely proneural, classical, neural, and mesenchymal with distinct gene expression signatures (Verhaak et al., 2010). The proneural subtype is highly enriched with the signature associated with oligodendrocyte lineage cells, whereas the classical subgroup is strongly associated with the astrocytic signature, and the mesenchymal subgroup is enriched with a gene signature associated with cultured/reactive astrocytes and microglia (Lei et al., 2011; Verhaak et al., 2010). Much of the heterogeneity of GBMs can be attributable to their distinct genetic alterations (Brennan et al., 2013; Carro et al., 2010). The proneural subtype displays characteristic genetic alterations including *PDGFRA* amplification and *TP53* mutations, as well as *IDH1* or *IDH2* mutations (Brennan et al., 2013; Verhaak et al., 2010), while the classical subtype is characterized by mutational activation *EGFR* or by extra copies of *EGFR* (Hayden, 2010). Although distinct events occurring in different target cells likely contribute to the variety of GBM phenotypes, the molecular determinants that regulate the tumor phenotype are not fully understood.

Depending on genetic alterations, glioma cells may transition between different states by utilizing alternative pathways that incite tumor growth and progression (Johnson et al., 2014; Meacham and Morrison, 2013). Since either activation of  $\text{TNF-}\alpha/\text{NF-}\kappa\text{B}$  or loss of *NF1* converts proneural GBM to the mesenchymal subtype (Bhat et al., 2013; Ozawa et al., 2014), GBM tumor cells therefore manifest phenotypic plasticity. This plasticity may render tumor cells more invasive or resistant to current therapies at different stages in their development (Friedmann-Morvinski et al., 2012; Persson et al., 2010). At present, the underlying genetic alterations and the signaling mechanisms that result in transitions between different tumor cell states remain elusive. Identification of the molecular control of tumorigenic cell properties and cellular hierarchies within GBM are essential for understanding pathogenic processes and may lead to potential avenues for targeted GBM treatment, especially with regard to confronting resistance.

Recent studies indicate that a population of stem-like tumor propagating cells appears to drive tumor growth and progression in GBM (Chen et al., 2012; Liu et al., 2011; Schonberg et al., 2014). OLIG2, an early marker for oligodendroglial lineage progenitors (Lu et al., 2002), is expressed in all grades of diffuse gliomas (Ligon et al., 2004). Remarkably, the proneural tumor subtype possesses a gene expression profile that resembles that of oligodendrocyte precursor cells (OPCs) (Lei et al., 2011; Liu et al., 2011; Verhaak et al., 2010), a presumptive cell type of origin for this type of GBM. Moreover, OLIG2 has been identified as one of core transcription factors that reprogram differentiated GBM cells into the stem-like propagating cells (Suva et al., 2014). Previous studies indicate that neural progenitors isolated from *Olig1/2*<sup>-/-</sup>; *Cdkn2a*<sup>-/-</sup> embryos cannot be induced by oncogenic *EGFRvIII* to form glioma in murine allografts (Ligon et al., 2007). In addition, Olig2 appears to directly oppose p53 responses to genotoxic damage to regulate glioma growth (Mehta et al., 2011). Currently, it is not clear whether Olig2 is required for endogenous glioma formation, particularly on a *Trp53*-mutant background, since p53 is one of the most frequently inactivated proteins in the development of malignant glioma or GBM in humans (Verhaak et al., 2010). The molecular mechanisms whereby Olig2 regulates glioma tumorigenesis are not fully understood. Furthermore, because Olig2<sup>+</sup> cells are present in most diffuse gliomas, whether Olig2<sup>+</sup> propagating cells are critical for directing tumor cell growth and progression in GBM remains unknown.

## Results

### Intense Olig2 expression characterizes mitotic progenitors in human and mouse gliomas

To characterize OLIG2 expression in mitotic progenitors in human proneural-like GBM with *PDGFRA* amplification, we performed immunostaining for OLIG2 and a proliferative marker, Ki67. We detected extensive OLIG2 expression in tumor lesions (Figure 1A). Approximately  $35 \pm 5\%$  of OLIG2<sup>+</sup> cells expressed Ki67 among the GBMs examined (Figures 1B and 1C), and substantial populations of OLIG2<sup>+</sup> cells were co-labeled with SOX2, POU3F2, or CD133 (Figures 1B and 1C), the markers for tumor initiating/propagating cells (Schonberg et al., 2014). These tumor propagation-associated markers were enriched on OLIG2<sup>+</sup> cell populations in GBM lesions (Figures S1A and S1B). Similarly, a large population of Ki67<sup>+</sup> cells expressed OLIG2 in proneural GBM (Figure S1C), which is consistent with previous findings (Ligon et al., 2007). These observations suggest OLIG2<sup>+</sup> cells are highly proliferative with tumor progenitor properties in proneural-like GBM lesions.

To investigate the role of Olig2<sup>+</sup> cells in glioma formation, we induced malignant gliomas in adult mice by deleting both floxed alleles of *Pten* and *Trp53* with a Cre-expressing retrovirus carrying PDGFB through stereotaxic microinjection into the cerebral white matter (Figure 1D) (Lei et al., 2011). This murine model of malignant glioma closely resembles the human proneural GBM (Lei et al., 2011). These tumors carry well-defined genetic alterations with PDGF pathway activation accompanied by *Trp53* and *Pten* losses, exhibiting pathological and morphological characteristics of human GBM (Figure S1D) (Lei et al., 2011; Sonabend et al., 2014). These mouse gliomas consisted of a large population of Olig2-expressing cells (Figure 1E), which were highly proliferative as indicated by Ki67 expression in approximately  $46 \pm 6\%$  of Olig2<sup>+</sup> cells (Figures 1F and 1I). The proportion of Ki67<sup>+</sup> proliferative cells among Olig2<sup>+</sup> cells was higher than that in Olig2<sup>-</sup> cells (Figures 1I and S1E). Similar to human proneural GBM, a substantial population of Olig2<sup>+</sup> cells expressed Sox2 and Pou3f2 (Figures 1G–1I and S1E). In addition, a large majority of Ki67<sup>+</sup> cells were Olig2-positive (Figure S1F), suggesting that Olig2<sup>+</sup> mitotic cells are a major component of the proliferating cell mass in this mouse glioma model.

### Ablation of mitotic Olig2<sup>+</sup> cells inhibits glioma formation and progression

To test whether Olig2<sup>+</sup> proliferative cells are the critical source of glioma growth, we utilized an in vivo cell suicide approach to deplete mitotic Olig2<sup>+</sup> progenitors by generating *Olig2-TK* (thymidine kinase) mice with the ganciclovir (GCV)-inducible suicide gene *HSV-TK* knocked-in at the *Olig2* locus (Figures 2A and 2B). TK expression in *Olig2-TK* knock-in mice mirrored Olig2 expression patterns (Figure 2C). HSV-TK kinase activity converts GCV into toxic triphosphates that inhibit DNA polymerase and eliminate actively dividing tumor cells, while sparing normal post-mitotic Olig2<sup>+</sup> cells like mature oligodendrocytes (Figures 2D, S2A and S2B). When GCV was administered to the glioma-forming mice carrying *Olig2-TK* at day 5 post PDGFB-Cre virus injection (dpi 5), tumor growth was markedly inhibited compared with control tumor-forming animals (*Pten<sup>fl/fl</sup>;Trp53<sup>fl/fl</sup>*;PDGFB-Cre; designated as Ctrl-T) (Figures 2E and 2F). GCV-treated *Olig2-TK* mice had a significantly extended survival curve relative to that of control tumor

mice (Figure 2E). Histologic analysis revealed that the majority of the *Olig2-TK* mice had no detectable tumor mass and exhibited few Ki67<sup>+</sup> proliferative cells in the brain compared with Ctrl-T mice (Figures 2F and 2G), suggesting that Olig2<sup>+</sup> mitotic cells represent a population of tumor cells that are necessary for tumor propagation in this animal model.

Even when GCV treatment was performed at dpi 20, a late phase of tumorigenesis, the gliomaforming *Olig2-TK* mice survived longer compared to control groups (Figure 2H). However, the survival rate was much reduced in the animal group administered GCV at dpi 20 compared to those treated earlier in tumorigenesis at dpi 5 (Figures 2E and 2H). We observed that the proportion of proliferative Olig2<sup>+</sup> cells decreased while the percentage of Olig2<sup>-</sup> cells among Ki67<sup>+</sup> cells increased in Ctrl-T tumors at dpi 23 compared with dpi 5 (Figures 2I and 2J). The increase in Olig2<sup>-</sup> proliferative cells suggests that both Olig2<sup>+</sup> and Olig2<sup>-</sup> mitotic cells are responsible for the tumor growth during the late stage of tumor progression.

### ***Olig2* deletion delays the growth and progression of glioma**

To determine the function of Olig2 in glioma formation, we bred floxed *Pten* and *Trp53* mice with mice carrying an *Olig2* floxed allele (Yue et al., 2006). Cre virus transduction will ablate the *Olig2*<sup>fl/fl</sup> allele together with *Pten* and *Trp53* floxed alleles in the same cells. The resulting animals with *Olig2* deletion (*Pten*<sup>fl/fl</sup>; *Trp53*<sup>fl/fl</sup>; *Olig2*<sup>fl/fl</sup>:PDGFB-Cre) are designated as *Olig2cKO*. In contrast to robust Olig2 expression in Ctrl-T tumors, Olig2 was essentially undetectable in Cre-expressing cells in *Olig2cKO* tumors (Figure S3A). Residual Olig2<sup>+</sup> cells observed in the *Olig2cKO* tumors were not Cre-retrovirus transduced (Figure S3A), and therefore they do not have Cre-mediated *Pten* and *Trp53* deletion; these cells might represent non-transformed OPCs that have been entrapped or recruited to the tumor.

To trace the growth and progression of tumors from Cre-recombined cells, we performed in vivo bioluminescence imaging of the Ctrl-T and *Olig2cKO* mice carrying the Rosa26-tmLuciferase reporter (Figure 3A). In the Ctrl-T mice with *Pten* and *Trp53* deletion, initial tumor formation was detected around dpi 15. Tumors grew rapidly and spread extensively in the brain over time as indicated by increasing luminescent signal (Figure 3A). Most control tumor-forming mice died before dpi 30 (Figure 3A). In contrast, in the *Olig2cKO* mice, we detected tumor appearance at a later stage around dpi 20. Intriguingly, tumor mass continued to expand before most *Olig2cKO* mice succumbed to the tumor by around dpi 50 (Figures 3A and 3B), indicating that *Olig2* ablation led to a slower rate of growth and/or a delay in tumor initiation. However, the size of tumors monitored by luminescent signals gradually increased and eventually reached a level resembling the control tumor groups at the terminal stage of tumor growth (Figure 3B).

Histological analyses of tumors confirmed glioma formation and growth across time-points post-viral injection in Ctrl-T and *Olig2cKO* mice (Figures 3C, S3B and S3C). The glioma in *Olig2cKO* mice in the end-stage tumors at dpi 40 was similar to that of control tumors (Figures S3C–S3E), resembling human GBM with characteristic high mitotic index and pseudopalisading necrosis. To examine the effect of *Olig2* ablation on tumor cell proliferation, we carried out BrdU pulse labeling of proliferating cells. In the *Olig2cKO* tumors, Olig2 expression in the neoplasm was essentially absent, although Sox2<sup>+</sup>/BrdU<sup>+</sup>

proliferative cells remained in the lesion (Figure 3D). The residual Olig2<sup>+</sup> cells expressed neither Sox2 nor BrdU, suggesting that they are not the major contributors to the continued, albeit slower, tumor growth in *Olig2*cKO mice (Figure 3D). The number of BrdU<sup>+</sup> cells was significantly reduced in the *Olig2*cKO tumors during the early stage of tumorigenesis (Figures 3E and 3F). In late-stage tumors, however, the BrdU labeling was comparable between the two groups (Figures 3E and 3F). Kaplan-Meier survival analysis indicated that *Olig2* deletion resulted in prolonged survival (Figure 3G), suggesting that *Olig2* deletion delays, but does not prevent, glioma initiation and progression.

### ***Olig2*-deleted tumor cells exhibit markedly reduced sphere-forming capacity but retain tumorigenic capacity**

To examine the self-renewal capacity of tumor cells in the absence of Olig2, we performed neurosphere formation assays. In contrast to Ctrl-T counterparts, which formed free-floating spheres, the *Olig2*-deleted tumor cells readily attached to form a monolayer culture (Figure 4A). Primary spheres were then dissociated and plated at clonal density over serial passages. The control tumor cells maintained their sphere formation capacity, whereas very few spheres were formed by *Olig2*cKO tumor cells during passages (Figures 4A and 4B). When tumor cells isolated from Ctrl-T and *Olig2*cKO neoplasms were plated as adherent monolayers in the same mitogenic conditions, the Olig2-deleted tumor cells were able to expand and proliferate, as assessed by BrdU incorporation, although these cells exhibited a lower proliferation rate than control tumor cells (Figures 4C and 4D).

We further analyzed the clonogenic capacity of *Olig2* mutant cells using the soft agar assay at clonal density. Ctrl-T and *Olig2*cKO tumor cells were able to form colonies and displayed similar clonogenicity; however, the overall sizes of colonies formed by *Olig2*cKO tumor cells were smaller than those of Ctrl-T cells over 20 days (Figures 4E–4G), suggesting a slower growth rate in *Olig2*cKO than control tumor cells. When cultured under neural differentiation conditions, Olig2<sup>+</sup> tumor spheres differentiated into PDGFRα<sup>+</sup> OPC-like cells along with a few GFAP-expressing cells (Figure 4H); in contrast, the vast majority of *Olig2*-deleted cells were predominantly differentiated into GFAP<sup>+</sup> astrocyte-like cells but not PDGFRα<sup>+</sup> OPC-like cells (Figure 4H), indicating that Olig2 is required for PDGFRα expression and maintenance of growth of PDGFRα<sup>+</sup> OPC-like cells, while suppressing astrocytic GFAP expression. Similarly, we detected an up-regulation of GFAP in *Olig2*cKO tumors (Figure S4A). *Olig2* deletion resulted in an increase of astroglial gene expression while causing a down-regulation of OPC-associated gene expression in cultured tumor cells (Figure S4B). This is consistent with Olig2 function in control of oligodendrocyte and astrocyte fate switch (Cai et al., 2007; Zhu et al., 2012).

To investigate the tumorigenic capacity of the cells derived from *Olig2*-deleted tumors in vivo, we performed orthotopic transplantation into the cerebral striatum of immunodeficient NOD *scid* gamma (NSG) mice, which were engrafted with  $1 \times 10^4$  or  $1 \times 10^3$  tumor cells. The cells transplanted from either Ctrl-T or *Olig2*cKO tumors formed secondary tumors that resembled their parental tumors histologically (Figure 5A). Kaplan-Meier survival analysis revealed prolonged survival of mice with secondary tumors derived from *Olig2*cKO tumors compared with those derived from Ctrl-T tumors (Figure 5B). To determine the growth rate



of *Olig2*KO tumor cells in the engrafted mice, we monitored bioluminescence for tumor development and found that *Olig2*-deletion stalled progression of tumorigenesis (Figure 5C), paralleling results in *Olig2*KO primary tumors. Similar to primary tumors, the residual *Olig2*<sup>+</sup> cells in transplanted *Olig2*KO tumors were not proliferative (Figures 5D and 5E) and were without Cre expression (data not shown), suggesting that these cells were non-transformed *Olig2*<sup>+</sup> cells residing within tumor lesions. Together, our data indicate that *Olig2*-deleted tumor cells maintain tumorigenic capacity despite a relatively slower growth rate.

### **Olig2 directly targets the enhancers of cell cycle regulators and oncogenes to regulate their expression**

To determine the mechanisms for *Olig2* regulation of tumor growth, we carried out transcriptome profiling of control and *Olig2*KO tumor tissues as well as normal adult cortical tissues using RNA-sequencing. By interrogating gene expression signatures from the Molecular Signatures Database (MSigDB) (Subramanian et al., 2005), we identified the pathways associated with tumorigenesis including DNA replication, oncogenic pathways and cell proliferation were substantially activated in Ctrl-T tumors comparing with normal cortex, while those pathways activities were downregulated in *Olig2*KO tumors (Figure 6A). Similarly, the genes down-regulated in *Olig2*KO tumors as compared to Ctrl-T tumors were related to the regulators of cell proliferation, survival, stemness and oncogenic programs (Figures 6B and 6C). These observations suggest that *Olig2* promotes tumorigenesis through controlling multiple oncogenic pathways.

To identify the genes directly regulated by *Olig2*, we performed whole-genome chromatin immunoprecipitation sequencing (ChIP-seq) using *Olig2*-expressing control tumors. The *Olig2*-targeted genes were highly enriched in the enhancer regions, marked by the activating histone mark H3K27ac, in the genome of tumor tissues (Figure 6D). When comparing the *Olig2* occupancy profiles with those of *Olig2*-enriched neural progenitor cells (NPCs) (Meijer et al., 2014), we detected a unique subset of gene promoters/enhancers exhibiting strong *Olig2* enrichment in the neoplasm but not in normal NPCs (Figure 6E). A cohort of *Olig2*-targeted sites was identified specifically in tumors (Figure 6F), but not in *Olig2*-enriched NPCs or OPCs (Yu et al., 2013). These sites are mainly associated with genes known to encode regulators of cell growth and proliferation such as cell cycle regulators *Cdca8*, *Cdc20*, *Cdc25c*, along with cell proliferation-promoting factors *Aurka* and *Pim1* (Figures 6G and 6H). Strikingly, we detected a strong enrichment of *Olig2* binding in the enhancer/promoter regions of oncogenic genes, marked by H3K27ac and H3K4me3, such as proto-oncogenes *Myc* and *Jun* (Figure 6H). Expression of these genes is required for maintenance of glioma stem cell growth (Wang et al., 2008), and has been shown to promote cell cycle progression and cellular proliferation (Nie et al., 2012).

To further confirm that expression of these target genes was dependent on *Olig2* expression in the tumors, we performed qPCR analysis and found that expression of the *Olig2*-targeted genes such as *Cdc20*, *Cdc25c*, *Aurka* and *Myc* were dramatically increased in the *Olig2*-expressing Ctrl-T tumors compared with the wild-type corpus callosum (Figure 6I). By contrast, transcripts from these cell cycle-promoting genes and proto-oncogenes c-Myc and

c-Jun were down-regulated in the *Olig2*KO tumors compared to Ctrl-T tumors (Figures 6J and 6K), suggesting that Olig2 transcriptionally targets the enhancers of the genes encoding the regulators of cell growth, and activates their expression to promote cell proliferation during tumorigenesis.

### **Loss of Olig2 leads to a proneural phenotype shift to an astroglia-associated classical-like gene expression pattern**

Given the persistent, but delayed, glioma formation in *Olig2*KO mice, we questioned whether alternative pathways sustain the growth and progression of *Olig2*-deleted tumors. We therefore compared the transcriptome profiles of Ctrl-T and *Olig2*KO tumors. We compared these profiles to those of validated subtypes of human GBM samples from the Cancer Genome Atlas Project (CGAT, 2008). Gene regulatory network analysis revealed that the genes that were highly enriched in Ctrl-T tumors were closely related to oligodendrogenesis and cell proliferation, and with those associated with the proneural subtype of GBM characterized by an oligodendrocytic gene expression pattern (Figures 7A and 7B). In contrast, the genes that were over-represented in *Olig2*KO tumors were correlated with astroglionogenesis and resembled the gene expression pattern of classical-like tumors (Figure 7B). These observations suggest that *Olig2* deletion leads to a tumor phenotype shift. By analyzing the expression level of signature genes identified in different GBM subtypes (Verhaak et al., 2010) between Ctrl-T and *Olig2*KO tumors, we found that *Olig2*-deletion led to downregulation of proneural signature genes and up-regulation of a set of classical signature genes (Figure 7C). Consistently, the gene sets enriched in Ctrl-T and *Olig2*KO tumors were over-represented in proneural and classical GBMs, respectively (Figure 7D).

To define potential glioma phenotype shift in an unbiased manner, we then performed Gene Set Enrichment Analysis (GSEA) (Subramanian et al., 2005) to compare the expression pattern of Ctrl-T and *Olig2*KO tumors with the datasets from four GBM subgroups (CGAT, 2008; Verhaak et al., 2010). Based on GSEA, the transcriptome profile of Ctrl-T tumors was a significant match to the signature of the proneural subtype of GBM (Figure 7E). In contrast, signature gene sets associated with classical GBM, but not mesenchymal or neural subtypes, were significantly enriched in the gene expression profile of *Olig2*KO tumors (Figure 7E).

qRT-PCR analysis further confirmed that expression of a set of astroglia-associated classical signature genes such as *Egfr*, *Tbx2*, *Gli2*, and *Jag1* was substantially increased in *Olig2*KO tumors (Figure 7F), whereas expression of proneural signature genes was downregulated. Expression of mesenchymal and neural signature genes was not significantly altered by *Olig2* deletion (Figure 7F). In addition, we found that Olig2 directly targets the regulatory regions of the classical signature genes including *Egfr*, *Tbx2*, and *Gli2* (Figure 7G). In *Olig2*KO tumors, the activating histone mark H3K27ac was significantly enriched in enhancer regions of these genes, which were correlated with up-regulation of their expression in the absence of Olig2 (Figure 7G). This suggests that Olig2 negatively regulates expression of these classical signature genes in glioma.



To determine whether Olig2 down-regulation at the cellular level results in a shift of gene expression patterns, we knocked down Olig2 with lenti-shRNA in Ctrl-T tumor cells in culture. qRT-PCR was used to examine expression of a set of proneural signature (e.g., *Olig2*, *Dll3*, *Ascl1*, *Slc1a1* and *Pdgfra*) and classical signature (e.g., *Egfr*, *Tbx2*, *Gli2*, and *Jag1*) genes (Verhaak et al., 2010). Strikingly, we found that the inhibition of Olig2 expression reduced proneural gene expression and led to an increase of expression in the classical signature genes such as *Egfr* compared to levels in control shRNA-treated cells (Figure 7H).

TCGA gene expression datasets and immunohistochemistry indicated that the tumors from the proneural GBM cohort of patients exhibit a high level of OLIG2 expression accompanied by a low level of EGFR expression, whereas a higher EGFR level was observed in the classical subtype cohort than in the proneural GBM cohort (Figures 7I, 7J, and S5A–S5C). This is in agreement with the previous observation that approximately 97% of patients with classical GBMs have high-level EGFR expression or amplification (Verhaak et al., 2010). Consistently, the proportion of OLIG2<sup>+</sup> or OLIG2<sup>+</sup>/PDGFRA<sup>+</sup> cells in GBM tissues was higher in the proneural group than the classical group (Figures S5D–S5F). There is a positive correlation between OLIG2 and PDGFRA expression among GBMs with *PDGFRA* amplification in TCGA datasets (Figure S5G), however, the levels of OLIG2 and EGFR expression are uncorrelated in TCGA core GBM samples. Although EGFR expression in OLIG2<sup>+</sup> cells appears variable, ranging from absent or low to high, we observed that the percentage of OLIG2<sup>+</sup> cells expressing low or absent EGFR was substantially higher than that of those with high EGFR expression in a cohort of proneural tumors (Figure S5H), consistent with a role of OLIG2 in repression of EGFR expression.

To further correlate OLIG2 down-regulation to gene expression changes, we knocked down expression of OLIG2 by shRNA in two primary human proneural GBM cell lines, TS543 and TS667; both lines characterized by *PDGFRA* amplification (Ozawa et al., 2014). We found that OLIG2 depletion by shRNA knockdown resulted in a reduction in the rate of cell proliferation as assayed by BrdU incorporation (Figures 7K and 7L). Similarly, OLIG2 knockdown in an OLIG2-expressing glioma cell line SU-AO2 with *IDH1* mutation (Venkatesh et al., 2015) also caused a decrease in cell proliferation (Figures S5I and S5J). Furthermore, expression of characteristic genes of classical GBM, including EGFR, were up-regulated, while PDGFRA expression was downregulated upon treatment of cells with the OLIG2-specific shRNA in TS543 and TS667 cells (Figure 7M). Collectively, these observations suggest that OLIG2 has a cell-autonomous role on the phenotype of tumor cells.

### Inhibition of EGFR signaling blocks *Olig2*-deleted tumor cell proliferation

We observed that *Egfr* was significantly up-regulated in *Olig2*KO tumors, and that Olig2 directly targets the regulatory elements of *Egfr* and represses *Egfr* expression (Figure 7G). These results point to EGFR signaling that sustains reduced tumorigenesis in the *Olig2*KO mice. Immunostaining and western blot analysis indicated robust EGFR up-regulation in *Olig2*KO tumors in contrast to weak EGFR expression in Ctrl-T tumors (Figures 8A–8D), while EGFR<sup>+</sup> cells in *Olig2*KO tumors were proliferative (Figure 8B). In *Olig2*KO

tumors, expression of the activated form EGFR, phospho-EGFR, was also up-regulated (Figures 8C and 8D). Similarly, downstream targets of EGFR signaling, p-Erk and p-Akt, were increased in *Olig2*-deleted tumors, whereas overall Erk and Akt levels were unchanged relative to those in Ctrl-T tumors (Figures S6A and S6B). Consistent with activation of EGFR signaling, expression of EGFR ligands including EGF, HB-EGF, and TGF $\alpha$  were detected in *Olig2*cKO tumor tissues and all human TCGA GBM tumor samples (Figures S6C and S6D).

In contrast to EGFR, levels of PDGFR $\alpha$  and phospho-PDGFR $\alpha$  were substantially downregulated in *Olig2*cKO tumors (Figures 8C and 8D). The number of PDGFR $\alpha$ -expressing cells was decreased in *Olig2*cKO relative to Ctrl-T tumor tissues (Figure 8E and 8F). In addition, we observed that Olig2 targets directly the enhancer regions of the *Pdgfra* gene locus in glioma (Figure S6E). Collectively, these observations suggest that Olig2 negatively regulates EGFR expression while activating PDGFR $\alpha$  expression in glioma.

Given that the EGFR pathway is activated in the *Olig2*-deleted tumors, we tested whether tumor cells with *Olig2* deletion were sensitive to inhibition of EGFR signaling by treating tumor cells derived from Ctrl-T and *Olig2*cKO tumors with gefitinib, an EGFR inhibitor (Cataldo et al., 2011). Gefitinib treatment exhibited a stronger inhibitory effect on the proliferation of *Olig2*cKO tumor cells than Ctrl-T tumor cells as assayed by BrdU incorporation (Figures 8G and 8H). Similar results were also observed upon treatment of cells with erlotinib, another EGFR inhibitor (Cataldo et al., 2011) (data not shown). The number of viable cells detected by CellTiter Glo assay (Noah et al., 2007) was reduced significantly in *Olig2*-deleted cells after treatment with gefitinib, while Olig2<sup>+</sup> Ctrl-T tumor cells were less sensitive to gefitinib treatment (Figure 8I). Furthermore, the number of cells undergoing apoptosis as marked by cleaved, active Caspase 3 was significantly higher in *Olig2*cKO cells in response to treatment than in Ctrl-T tumor cells (Figures 8J and 8K), where the majority of cleaved Caspase 3<sup>+</sup> cells did not express Olig2 (Figures S6F and S6G). These data indicated that the growth of *Olig2*cKO cells is more sensitive to the EGFR inhibition than that of Olig2-expressing Ctrl-T tumor cells. The loss of Olig2 resulted in substantial reduction of PDGFR $\alpha$  but not PDGFR $\beta$ , which exhibited a low level in control tumors (Figures S6H–6J). We found that inhibition of PDGFR signaling with crenolanib had no significant effect on the growth of *Olig2*cKO tumor cells (Figures S6K and S6L). This suggests that in the absence of Olig2, tumor cells likely acquire the alternative EGFR signaling pathway to maintain the growth at a reduced rate.

Next, to determine the in vivo effects of gefitinib treatment on the tumor growth of Ctrl-T and *Olig2*cKO mice, we initiated drug treatment 5 days after PDGFB-Cre retrovirus induction of tumorigenesis. Ctrl-T mice that received gefitinib exhibited an insignificant reduction in the tumor size compared to mice that received vehicle as assayed bioluminescent intensity (Figures 8L and 8N). In contrast, *Olig2*cKO mice treated with gefitinib showed a significant reduction in bioluminescence over the course of treatment compared with mice treated with DMSO, indicating that gefitinib treatment substantially delayed tumor growth (Figures 8M and 8N). Gefitinib treatment resulted in a significant increase in survival time of the *Olig2*cKO animals (Figure 8O), suggesting that *Olig2*

depletion sensitizes glioma cells to EGFR signaling inhibition and improved animal lifespans.

## Discussion

In the present study, we demonstrate that mitotic Olig2-expressing cells are essential for tumor propagation in a murine model of proneural-subtype GBM, highlighting the dependency of brain tumorigenesis on Olig2<sup>+</sup> mitotic cells. Our findings also indicate that Olig2 reciprocally regulates distinct growth receptor PDGFR and EGFR signaling pathways and maintains tumor phenotype identity. Integrative analyses of genome occupancy and transcriptome profiling reveal that Olig2 directly activates a specific subset of genes that promote cell proliferation and oncogenic processes in the neoplasm distinct from normal NPCs. *Olig2* deletion leads to a significant delay in the onset and progression of glioma and causes a phenotype shift from an oligodendrocyte-lineage correlated proneural toward a astroglial gene expression pattern with activation of EGFR signaling. Our data indicate a critical role for Olig2 in regulating the growth rate and phenotypic plasticity of both mouse and human glioma cells. We further find that *Olig2* deletion results in sensitization of glioma cells to EGFR inhibition. Thus, our findings suggest a rationale for blocking Olig2-expressing proneural glioma growth through inhibiting Olig2 activity, and proof of principle to targeting tumor-propagating cells for stratifying therapy among distinct subtypes of malignant gliomas.

A previous study showed that Olig1/2-null cells were unable to form tumors in an allograft model in the presence of p53 (Ligon et al., 2007). Tumor cells however in our mouse model, which harbors deletions of *Trp53* and *Pten*, the most frequently mutated genes in GBM patients (Brennan et al., 2013; Verhaak et al., 2010), are able to continue to grow in the absence of Olig2, albeit at a slower rate, revealing a context-dependent function of Olig2 in brain tumorigenesis. Olig2 has been shown to repress cell cycle inhibitor p21<sup>WAF1/CIP1</sup> (Ligon et al., 2007) on the wild-type p53 background, and the requirement of Olig2 for tumor growth appears to be p53 dependent (Mehta et al., 2011). In the *Trp53/Pten* mutant glioma model, however, *Olig2* deletion leads to up-regulation of EGFR but not p21 (data not shown). This is in keeping with the lack of the reciprocal relationship between Olig2 and p21 expression in glioma cells carrying mutated or amplified EGFR (Mehta et al., 2011). Strikingly, our integrative genome occupancy and expression profiling analyses reveal that Olig2 directly activates regulators of cell cycle and oncogenic factors in tumors but not normal NPCs, suggesting that Olig2 acts as an accelerator of cell division during tumorigenesis. Our findings indicate that regulation of cell proliferation and oncogenic pathways by Olig2 is required for full tumorigenic potential and rapid cell expansion during tumor growth.

*Olig2*-deleted tumor cells exhibit increased adhesiveness, astrocytic phenotypes, and a defect in neurosphere formation, suggesting that Olig2 is required for the robust self-renewal of tumor propagating cells, consistent with the finding of Olig2 as a key transcription factor that drives GBM (Suva et al., 2014). A recent study indicates that self-renewal capacity, as measured by an in vitro sphere formation assay, does not determine the tumor growth potential of high-grade glioma (Barrett et al., 2012). Consistent with this, our data show that,

despite vastly diminished sphere formation capacity, *Olig2*-deleted cells are able to establish and form glioma, albeit at a decelerated rate. Together, our data suggest that *Olig2* promotes the growth of tumor cells through activation of cell-proliferation activating factors and maintenance of the proliferation potential of glioma cells.

Recent studies indicate that TNF- $\alpha$ /NF- $\kappa$ B signaling promotes mesenchymal differentiation of proneural GBM cells in vitro (Bhat et al., 2013). Additional *NFI* loss in a proneural glioma model induces proneural to mesenchymal transition (Ozawa et al., 2014). The molecular determinants that steer proneural subtype differentiation other than the mesenchymal lineage remain elusive. Gene profiling analysis indicates that *Olig2*-deleted tumors exhibit an increased expression of the gene signature of astrocytic classical-like GBM. In addition, *Olig2* knockdown in mouse tumor cells or human proneural GBM cells results in increased expression of a set of classical signature genes including EGFR. Thus, although we could not completely exclude the possibility of a change in tumor cell compositions or microenvironment, these observations suggest that the phenotypic shift of *Olig2*KO tumors occurs, at least in part, through a cell-autonomous effect of *Olig2* loss.

*Olig2*-expressing control tumor cells are highly enriched in oligodendrocyte lineage signatures, whereas the *Olig2*KO tumor cells were characterized by up-regulated expression of astroglial signature genes. This is consistent with the role of *Olig2* in suppressing the astroglial phenotype by inhibiting expression of GFAP and astrogenic factors such as NFIA (Cai et al., 2007; Glasgow et al., 2014). Our observation of an apparent shift toward “classical” from “proneural” expression patterns based on the TCGA classification of gliomas likely reflects a switch from an oligodendroglial to astroglial gene expression pattern in the absence of *Olig2*. It is worth noting that *Olig2* deletion does not necessarily cause a GBM subtype conversion. Rather, *Olig2* deletion leads to a transcriptional program shift with apparent up-regulation of astroglia-correlated signature genes, while downregulation of oligodendrocyte precursor-associated proneural gene expression in our animal model.

*Olig2*<sup>+</sup> mitotic cell elimination virtually abrogates tumor growth in our animal model of proneural-subtype gliomas, suggesting mitotic *Olig2*-expressing cells as a seeding source for proneural glioma growth. Although the potential role of mitotic *Olig2*<sup>+</sup> cells in other subtype tumors remains to be determined, targeted elimination of OLIG2<sup>+</sup> mitotic cells will be beneficial for treatment of a set of malignant GBM, especially for the proneural tumors that are enriched in mitotic OLIG2<sup>+</sup> propagating cells. Notably, *IDH1* or *IDH2*-mutant gliomas are highly enriched for OLIG2. *IDH1/2* mutations cause a global DNA hypermethylation phenotype referred to as G-CIMP (Glioma CpG Island Methylator Phenotype) and widespread gene silencing (Brennan et al., 2013). Compared with other OLIG2-expressing non-G-CIMP tumors, *IDH*-mutant tumors are less aggressive (Joseph et al., 2013), raising a possibility of a context-dependent role of OLIG2 in tumor growth. Nonetheless, OLIG2 knockdown in *IDH1*-mutant SU-AO2 glioma cells results in a reduction of cell proliferation, suggesting that OLIG2 may also act as an oncogenic factor for the cell growth in *IDH*-mutant glioma. Collectively, our findings suggest that *Olig2* controls glioma phenotype plasticity and that targeted inhibition of *Olig2* sensitizes tumor cells to EGFR inhibition. The profound impact of targeting *Olig2* and EGFR signaling on glioma formation illuminates an

alternative avenue to stratify GBM treatment with tailored pharmacological intervention, to inhibit the growth of these highly lethal malignant brain tumors.

## EXPERIMENTAL PROCEDURES

### Animals, tissue samples, and Immunohistochemistry

Mouse lines, breeding and tissue processing used in this study are described previously (Yue et al., 2006) and in Supplemental Information. All animal experiments were approved by and performed according to the guidelines of the Institutional Animal Care and Use Committee at the Cincinnati Children's Hospital Medical Center, USA. Human PN-like subtype GBM tissues with *PDGFRA*-amplification and CL-like subtype GBM tissues with *EGFR* amplification, *CDKN2A* deletion and *PTEN* deletion were from the University of Cincinnati, the Cincinnati Children's Hospital Medical Center and Sichuan University. All human glioma samples were obtained with consent as outlined by institutional review boards at the individual Universities. Tissue processing and immunostaining procedures and antibodies used are listed in the Supplemental Information.

### Tumor Induction and Intracranial Transplantation

Gliomas induced by PDGFB-IRES-Cre retrovirus and bioluminescence imaging in the *Pten<sup>fl/fl</sup>;Trp53<sup>fl/fl</sup>* mice were described previously (Lei et al., 2011) and in the Supplemental Information.

### Drug Infusion

Mice were anaesthetized five days after PDGFB-Cre retrovirus injection, and implanted with osmotic minipump (Model 2004; Alzet-Direct Corp.) and cannulas (Brain Infusion Kit 3; Alzet-Direct Corp.). The infusion cannula was implanted through the same needle tract used for virus injection by the stereotaxic apparatus. The osmotic minipumps were filled up with vehicle (DMSO) or gefitinib (80 mg/ml) (flow rate 0.25  $\mu$ l/hr, resulting in delivery of 480  $\mu$ g/d) and were connected to the infusion cannulas.

### Cell Culture, RNA-seq, ChIP-seq, and Data Analysis

Tumor cell isolation, culture, and sphere formation assays were described in the Supplemental Information. RNA isolation, RNA-seq, ChIP-seq and data analyses were performed as described previously (Yu et al., 2013). Full details can be found in the Supplemental Information.

### Statistical Analysis

Statistical analyses were done using Microsoft Excel or Prism GraphPad 6.00 with Student's two-tailed *t* test for comparing two sets of data. One-way analysis of variance analysis (ANOVA) with a Newman-Keuls multiple comparison test for post-hoc analysis. Two-sided log-rank test was used to determine statistical significance of Kaplan-Meier survival curves.  $p < 0.05$  is considered to be statistically significant (Supplemental Information).

## Supplementary Material

Refer to Web version on PubMed Central for supplementary material.

## Acknowledgments

The authors would like to thank Xian Yao Zhou, Zhixing Ma, Jason Lu, Xiaoting Zhu, and Peter Sims for technical support. We thank Dr. Michelle Monje Deisseroth for providing SU-AO2 tumor cell lines, and Drs. Yi Zheng, Charles Stiles, Susan Wells and Edward Hurlock for critical comments. This study was funded in part by grants from the National Institutes of Health (R01 NS078092 and R01 NS075243) to QRL.

## References

- Barrett LE, Granot Z, Coker C, Iavarone A, Hambardzumyan D, Holland EC, Nam HS, Benezra R. Self-renewal does not predict tumor growth potential in mouse models of high-grade glioma. *Cancer Cell*. 2012; 21:11–24. [PubMed: 22264785]
- Bhat KP, Balasubramanian V, Vaillant B, Ezhilarasan R, Hummelink K, Hollingsworth F, Wani K, Heathcock L, James JD, Goodman LD, et al. Mesenchymal differentiation mediated by NF-kappaB promotes radiation resistance in glioblastoma. *Cancer Cell*. 2013; 24:331–346. [PubMed: 23993863]
- Brennan CW, Verhaak RG, McKenna A, Campos B, Nounmehr H, Salama SR, Zheng S, Chakravarty D, Sanborn JZ, Berman SH, et al. The somatic genomic landscape of glioblastoma. *Cell*. 2013; 155:462–477. [PubMed: 24120142]
- Cai J, Chen Y, Cai WH, Hurlock EC, Wu H, Kernie SG, Parada LF, Lu QR. A crucial role for Olig2 in white matter astrocyte development. *Development*. 2007; 134:1887–1899. [PubMed: 17428828]
- Carro MS, Lim WK, Alvarez MJ, Bollo RJ, Zhao X, Snyder EY, Sulman EP, Anne SL, Doetsch F, Colman H, et al. The transcriptional network for mesenchymal transformation of brain tumours. *Nature*. 2010; 463:318–325. [PubMed: 20032975]
- Cataldo VD, Gibbons DL, Perez-Soler R, Quintas-Cardama A. Treatment of non-small-cell lung cancer with erlotinib or gefitinib. *N Engl J Med*. 2011; 364:947–955. [PubMed: 21388312]
- CGAT. Comprehensive genomic characterization defines human glioblastoma genes and core pathways. *Nature*. 2008; 455:1061–1068. [PubMed: 18772890]
- Chen J, Li Y, Yu TS, McKay RM, Burns DK, Kernie SG, Parada LF. A restricted cell population propagates glioblastoma growth after chemotherapy. *Nature*. 2012; 488:522–526. [PubMed: 22854781]
- Friedmann-Morvinski D, Bushong EA, Ke E, Soda Y, Marumoto T, Singer O, Ellisman MH, Verma IM. Dedifferentiation of neurons and astrocytes by oncogenes can induce gliomas in mice. *Science*. 2012; 338:1080–1084. [PubMed: 23087000]
- Glasgow SM, Zhu W, Stolt CC, Huang TW, Chen F, LoTurco JJ, Neul JL, Wegner M, Mohila C, Deneen B. Mutual antagonism between Sox10 and NFIA regulates diversification of glial lineages and glioma subtypes. *Nat Neurosci*. 2014; 17:1322–1329. [PubMed: 25151262]
- Hayden EC. Genomics boosts brain-cancer work. *Nature*. 2010; 463:278. [PubMed: 20090720]
- Jansen M, Yip S, Louis DN. Molecular pathology in adult gliomas: diagnostic, prognostic, and predictive markers. *Lancet Neurol*. 2010; 9:717–726. [PubMed: 20610347]
- Johnson BE, Mazar T, Hong C, Barnes M, Aihara K, McLean CY, Fouse SD, Yamamoto S, Ueda H, Tatsuno K, et al. Mutational analysis reveals the origin and therapy-driven evolution of recurrent glioma. *Science*. 2014; 343:189–193. [PubMed: 24336570]
- Joseph NM, Phillips J, Dahiya S, M MF, Tihan T, Brat DJ, Perry A. Diagnostic implications of IDH1-R132H and OLIG2 expression patterns in rare and challenging glioblastoma variants. *Mod Pathol*. 2013; 26:315–326. [PubMed: 23041832]
- Lei L, Sonabend AM, Guarnieri P, Soderquist C, Ludwig T, Rosenfeld S, Bruce JN, Canoll P. Glioblastoma models reveal the connection between adult glial progenitors and the proneural phenotype. *PLoS One*. 2011; 6:e20041. [PubMed: 21625383]



- Ligon KL, Alberta JA, Kho AT, Weiss J, Kwaan MR, Nutt CL, Louis DN, Stiles CD, Rowitch DH. The oligodendroglial lineage marker OLIG2 is universally expressed in diffuse gliomas. *J Neuropathol Exp Neurol*. 2004; 63:499–509. [PubMed: 15198128]
- Ligon KL, Huillard E, Mehta S, Kesari S, Liu H, Alberta JA, Bachoo RM, Kane M, Louis DN, Depinho RA, et al. Olig2-regulated lineage-restricted pathway controls replication competence in neural stem cells and malignant glioma. *Neuron*. 2007; 53:503–517. [PubMed: 17296553]
- Liu C, Sage JC, Miller MR, Verhaak RG, Hippenmeyer S, Vogel H, Foreman O, Bronson RT, Nishiyama A, Luo L, et al. Mosaic analysis with double markers reveals tumor cell of origin in glioma. *Cell*. 2011; 146:209–221. [PubMed: 21737130]
- Lu QR, Sun T, Zhu Z, Ma N, Garcia M, Stiles CD, Rowitch DH. Common developmental requirement for Olig function indicates a motor neuron/oligodendrocyte connection. *Cell*. 2002; 109:75–86. [PubMed: 11955448]
- Meacham CE, Morrison SJ. Tumour heterogeneity and cancer cell plasticity. *Nature*. 2013; 501:328–337. [PubMed: 24048065]
- Mehta S, Huillard E, Kesari S, Maire CL, Golebiowski D, Harrington EP, Alberta JA, Kane MF, Theisen M, Ligon KL, et al. The central nervous system-restricted transcription factor Olig2 opposes p53 responses to genotoxic damage in neural progenitors and malignant glioma. *Cancer Cell*. 2011; 19:359–371. [PubMed: 21397859]
- Meijer DH, Sun Y, Liu T, Kane MF, Alberta JA, Adelmant G, Kupp R, Marto JA, Rowitch DH, Nakatani Y, et al. An amino terminal phosphorylation motif regulates intranuclear compartmentalization of Olig2 in neural progenitor cells. *The Journal of neuroscience : the official journal of the Society for Neuroscience*. 2014; 34:8507–8518. [PubMed: 24948806]
- Nie Z, Hu G, Wei G, Cui K, Yamane A, Resch W, Wang R, Green DR, Tessarollo L, Casellas R, et al. c-Myc is a universal amplifier of expressed genes in lymphocytes and embryonic stem cells. *Cell*. 2012; 151:68–79. [PubMed: 23021216]
- Noah JW, Severson W, Noah DL, Rasmussen L, White EL, Jonsson CB. A cell-based luminescence assay is effective for high-throughput screening of potential influenza antivirals. *Antiviral Res*. 2007; 73:50–59. [PubMed: 16904762]
- Ohgaki H, Kleihues P. Epidemiology and etiology of gliomas. *Acta neuropathologica*. 2005; 109:93–108. [PubMed: 15685439]
- Ozawa T, Riester M, Cheng YK, Huse JT, Squatrito M, Helmy K, Charles N, Michor F, Holland EC. Most human non-GCIMP glioblastoma subtypes evolve from a common proneural-like precursor glioma. *Cancer Cell*. 2014; 26:288–300. [PubMed: 25117714]
- Persson AI, Petritsch C, Swartling FJ, Itsara M, Sim FJ, Auvergne R, Goldenberg DD, Vandenberg SR, Nguyen KN, Yakovenko S, et al. Non-stem cell origin for oligodendroglioma. *Cancer Cell*. 2010; 18:669–682. [PubMed: 21156288]
- Schonberg DL, Lubelski D, Miller TE, Rich JN. Brain tumor stem cells: Molecular characteristics and their impact on therapy. *Mol Aspects Med*. 2014; 39:82–101. [PubMed: 23831316]
- Sonabend AM, Bansal M, Guarnieri P, Lei L, Amendolara B, Soderquist C, Leung R, Yun J, Kennedy B, Sisti J, et al. The transcriptional regulatory network of proneural glioma determines the genetic alterations selected during tumor progression. *Cancer Res*. 2014; 74:1440–1451. [PubMed: 24390738]
- Subramanian A, Tamayo P, Mootha VK, Mukherjee S, Ebert BL, Gillette MA, Paulovich A, Pomeroy SL, Golub TR, Lander ES, et al. Gene set enrichment analysis: a knowledge-based approach for interpreting genome-wide expression profiles. *Proc Natl Acad Sci U S A*. 2005; 102:15545–15550. [PubMed: 16199517]
- Suva ML, Rheinbay E, Gillespie SM, Patel AP, Wakimoto H, Rabkin SD, Riggi N, Chi AS, Cahill DP, Nahed BV, et al. Reconstructing and reprogramming the tumor-propagating potential of glioblastoma stem-like cells. *Cell*. 2014; 157:580–594. [PubMed: 24726434]
- Venkatesh HS, Johung TB, Caretti V, Noll A, Tang Y, Nagaraja S, Gibson EM, Mount CW, Polepalli J, Mitra SS, et al. Neuronal Activity Promotes Glioma Growth through Neuroligin-3 Secretion. *Cell*. 2015; 161:803–816. [PubMed: 25913192]
- Verhaak RG, Hoadley KA, Purdom E, Wang V, Qi Y, Wilkerson MD, Miller CR, Ding L, Golub T, Mesirov JP, et al. Integrated genomic analysis identifies clinically relevant subtypes of

glioblastoma characterized by abnormalities in PDGFRA, IDH1, EGFR, and NF1. *Cancer Cell*. 2010; 17:98–110. [PubMed: 20129251]

Wang J, Wang H, Li Z, Wu Q, Lathia JD, McLendon RE, Hjelmeland AB, Rich JN. c-Myc is required for maintenance of glioma cancer stem cells. *PLoS One*. 2008; 3:e3769. [PubMed: 19020659]

Yu Y, Chen Y, Kim B, Wang H, Zhao C, He X, Liu L, Liu W, Wu LM, Mao M, et al. Olig2 targets chromatin remodelers to enhancers to initiate oligodendrocyte differentiation. *Cell*. 2013; 152:248–261. [PubMed: 23332759]

Yue T, Xian K, Hurlock E, Xin M, Kernie SG, Parada LF, Lu QR. A critical role for dorsal progenitors in cortical myelination. *J Neurosci*. 2006; 26:1275–1280. [PubMed: 16436615]

Zhu X, Zuo H, Maher BJ, Serwanski DR, LoTurco JJ, Lu QR, Nishiyama A. Olig2-dependent developmental fate switch of NG2 cells. *Development*. 2012; 139:2299–2307. [PubMed: 22627280]

### Significance

Distinct molecular characteristics in gliomas represent a significant hurdle for effective therapy. Here we uncover that a population of mitotic Olig2<sup>+</sup> cells is critical for initiation and progression of mouse primary gliomas. Intriguingly, deletion of *Olig2* results in tumors that exhibit persistent but decelerated growth. We find that Olig2 directly activates the transcriptional program for oncogenic growth. *Olig2* deletion engenders a tumor phenotype shift from a proneural to an astrocytic gene expression pattern, with PDGF receptor-alpha down-regulation and reciprocal EGFR signaling upregulation. Down-regulation of Olig2 sensitizes glioma cells to EGFR inhibition. Our observations reveal that Olig2 is a molecular arbiter of tumor phenotype plasticity that may underlie drug resistance, suggesting new strategies for enhancing EGFR drug sensitivity in glioma treatment.

**Highlights**

1. Elimination of mitotic Olig2<sup>+</sup> cells inhibits glioma initiation and progression
2. *Olig2* loss reduces glioma growth and causes proneural-to-astrocytic phenotype shift
3. *Olig2* deletion causes PDGFR down-regulation and reciprocal EGFR up-regulation
4. Inactivation of Olig2 potentiates sensitization of glioma cells to EGFR inhibition

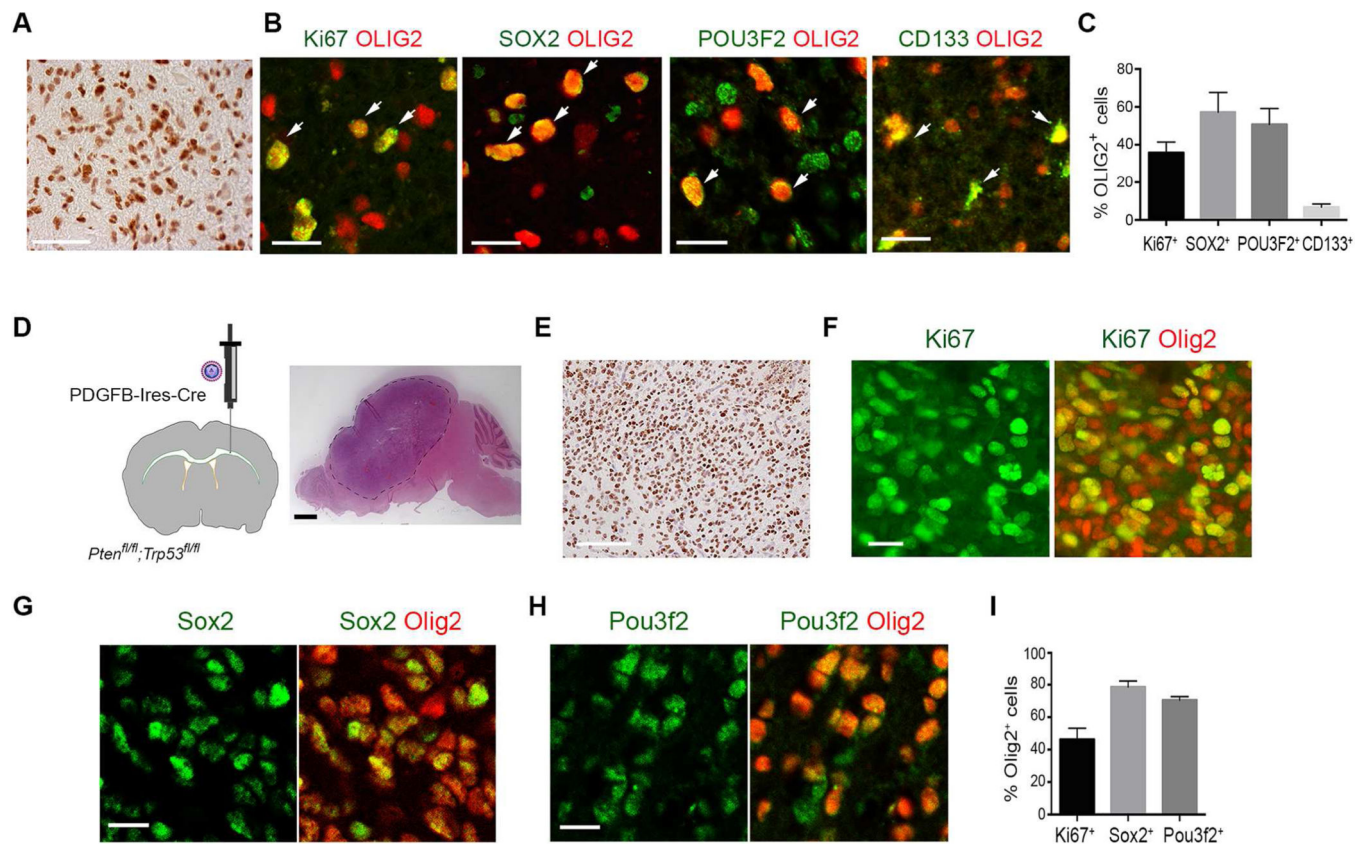


**Figure 1. Olig2 expression in mitotic progenitors in human and mouse GBM**

(A) A representative image showing OLIG2 (brown) expression in human proneural (PN) GBMs.

(B) Human PN GBM sections immunostained with OLIG2 (red) and Ki67, SOX2, POU3F2, or CD133 as indicated (green). Arrows indicate co-labeled cells.

(C) The percentage of labeling-positive cells among OLIG2<sup>+</sup> cells in proneural GBMs (n = 6 individual tumors; > 250 cell counts/tumor tissue).

(D) Left: PDGFB-Cre retrovirus injection into the cerebral white matter of 8-week old adult *Pten<sup>fl/fl</sup>; Trp53<sup>fl/fl</sup>* mice. Right: Hematoxylin and eosin (H&E)-stained brain section showing malignant glioma at dpi 24.

(E) Olig2 expression (brown) in PDGFB-Cre-induced glioma lesion.

(F–H) Glioma lesions were immunostained with Olig2 (red) and (F) Ki67, (G) Sox2, or (H) Pou3f2 (green).

(I) The percentage of co-labeled cells among Olig2<sup>+</sup> cells in tumor lesions. (n = 5 animals; > 250 cell counts/tumor tissue).

Scale bars in A–B, E–H, 50  $\mu$ m; D, 1 mm. Data are presented as mean  $\pm$  S.E.M. in C and I.

See also Figure S1.

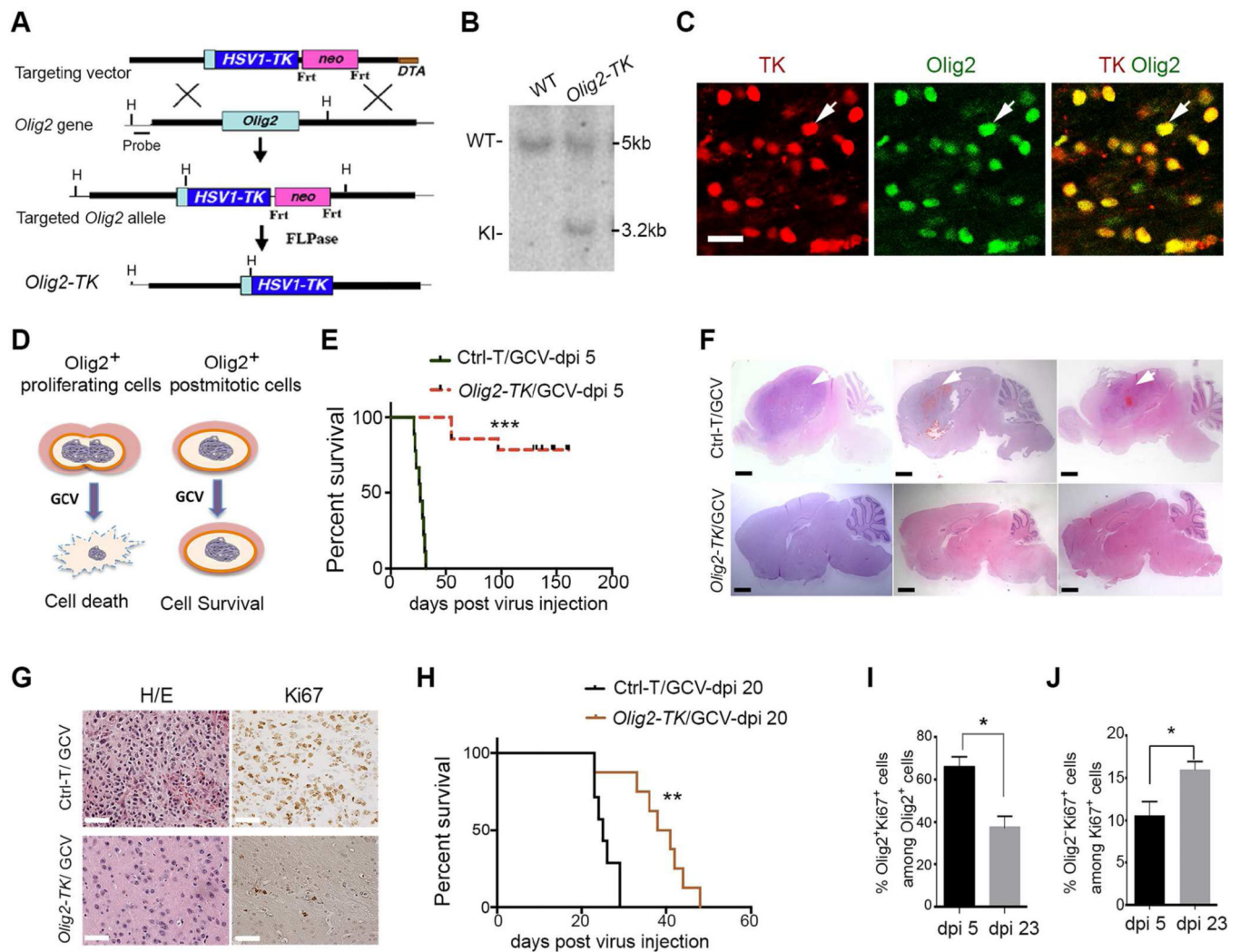


**Figure 2. Ablation of mitotic *Olig2*<sup>+</sup> cells inhibits glioma formation**

(A) Schematic design for *Olig2-TK* knock-in mice. The line below the *Olig2* locus represents the 5' external probe for Southern analysis. H, HindIII site; neo, neomycin cassette; Frt, flippase recognition targets; *DTA*, diphtheria toxin gene.

(B) Southern blot analysis of *Olig2-TK* knock-in with 5' *Olig2* probe using HindIII digested DNA. The 3.2 and 5-kb bands correspond to the knock-in and wild-type alleles, respectively.

(C) Immunostaining of TK and *Olig2* in the cortex of P14 *Olig2-TK* mice. Arrows: co-labeled cells.

(D) Schematic diagram showing GCV-mediated depletion of dividing *Olig2-TK*<sup>+</sup> cells that spares post-mitotic *Olig2*<sup>+</sup> cells.

(E) Kaplan-Meier survival analysis of GCV-treated control (n = 13) and *Olig2-TK* (n = 14) mice from dpi 5 (\*\*\* p < 0.001 with the log-rank test).

(F) H&E-stained brain sections from GCV-treated control and *Olig2-TK* mice. Arrows: tumor lesions.

(G) H&E and Ki67 staining of GCV-treated Ctrl-T mice (top panels) and *Olig2-TK* mice (bottom panels).



(H) Survival analysis of mice treated with GCV starting from dpi 20. Median survival in control group 25 days (n = 7) and in *Olig2-TK* group (n = 8) 39.5 days (\*\* p < 0.01 with the log-rank test).

(I, J) The percentage of Olig2<sup>+</sup>/Ki67<sup>+</sup> cells among Olig2<sup>+</sup> cells (I) and of Olig2<sup>-</sup>/Ki67<sup>+</sup> cells among Ki67<sup>+</sup> cells (J) in control tumors at dpi 5 and dpi 23. Data represent the means ± SEM in tumor tissues from three animals (> 250 cell counts/tumor tissue; \* p < 0.05; Student's *t* test).

Scale bars in C and G, 50 μm; F, 1 mm. See also Figure S2.

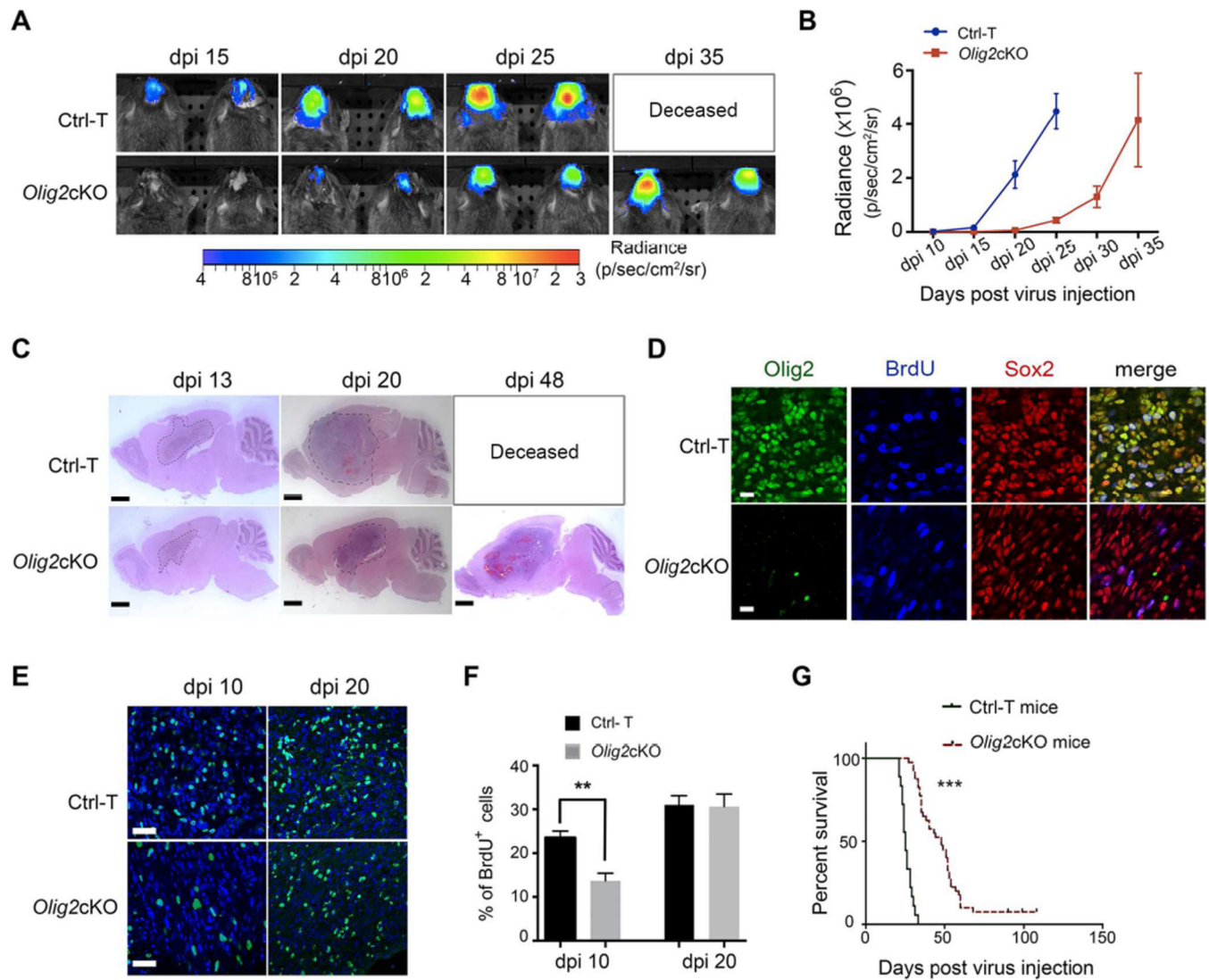


**Figure 3. *Olig2* deletion inhibits the growth of mouse glioma**

(A) Representative bioluminescence images of Ctrl-T and *Olig2cKO* mice during tumor progression.

(B) Quantification of bioluminescence signals as a function of time for Ctrl-T and *Olig2cKO* mice. Data are the means  $\pm$  SEM (n = 6 animals).

(C) H&E staining of brain sections of Ctrl-T and *Olig2cKO* tumors at dpi 13, 20, and 48.

(D) Sections of Ctrl-T and *Olig2cKO* tumors at dpi 13 were immunostained with Olig2, BrdU, and Sox2 after a 2-hr BrdU pulse labeling.

(E) Sections of Ctrl-T and *Olig2cKO* tumors at dpi 10 and dpi 20 immunostained for BrdU (green) after a 2-hr BrdU pulse labeling. DAPI in blue.

(F) Percentage of BrdU<sup>+</sup> cells in Ctrl-T and *Olig2cKO* tumors at dpi 10 and dpi 20. Data represent the means  $\pm$  SEM from three independent experiments (\*\* p < 0.01; Student's *t* test).

(G) Survival analysis of Ctrl-T and *Olig2cKO* mice. Median survival in Ctrl-T group (n = 18): 25 days; in *Olig2cKO* group (n = 37): 48 days (\*\*\* p < 0.001 with the log-rank test).

Scale bars in C, 1 mm; D, 20  $\mu$ m. E, 50  $\mu$ m. See also Figure S3.

Author Manuscript

Author Manuscript

Author Manuscript

Author Manuscript

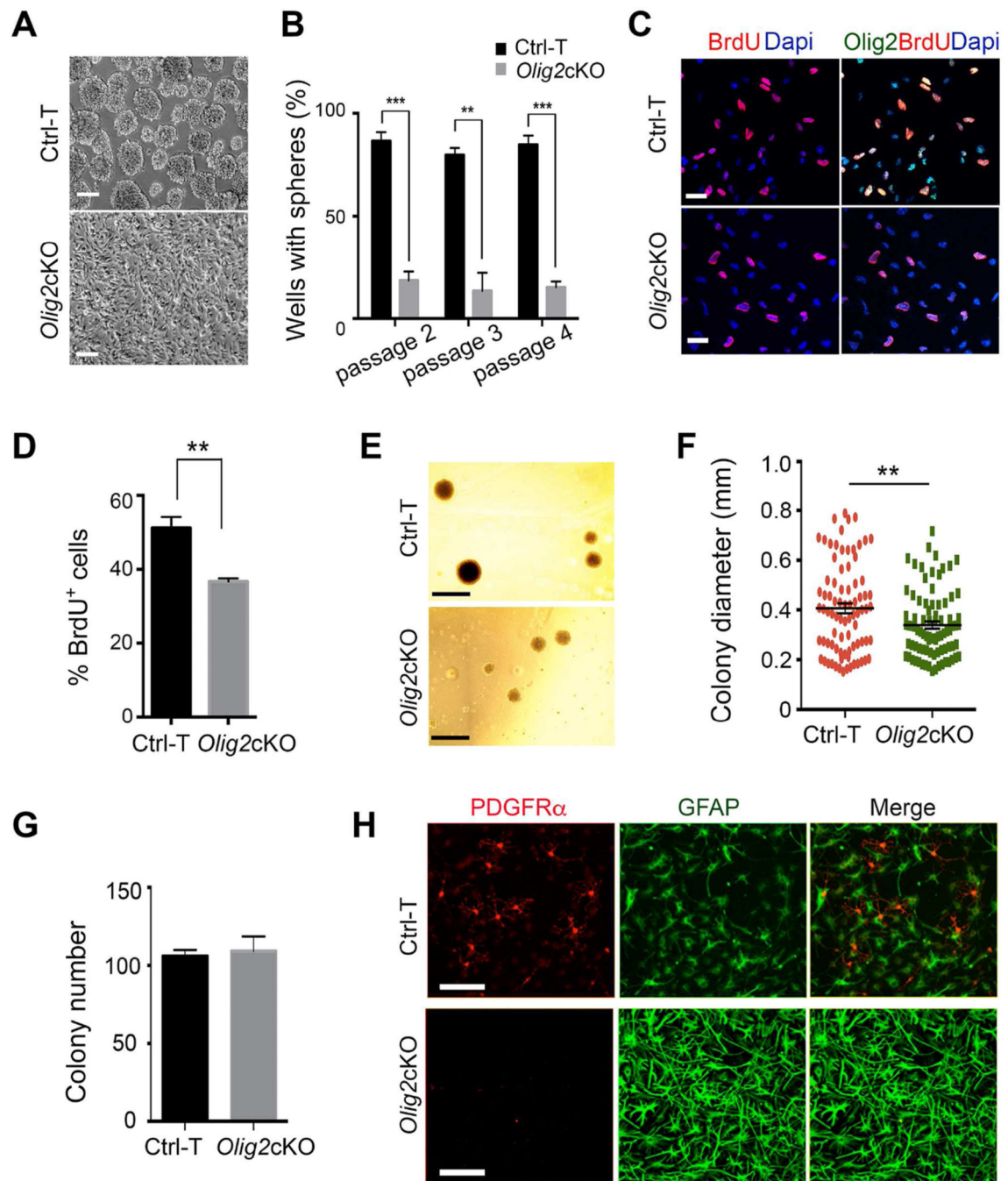


**Figure 4. Proliferation and differentiation of *Olig2cKO* tumor cells**

(A) Neurosphere formation from Ctrl-T and *Olig2cKO* tumor cells in serum-free media. Scale bar, 50  $\mu$ m.

(B) Percentage of wells that formed spheres from Ctrl-T and *Olig2cKO* tumor cells at clonal density in continuous passages.

(C) Ctrl-T and *Olig2cKO* tumor cell cultures were pulse-labeled with BrdU for 1 hr and immunostained with BrdU and Olig2 and counterstained with DAPI. Scale bar, 20  $\mu$ m.

(D) Percentage of BrdU<sup>+</sup> Ctrl-T and *Olig2cKO* tumor cells pulse-labeled with BrdU for 1 hr.

(E) Representative images of soft agar colony formation by Ctrl-T and *Olig2*KO tumor cells. Scale bar, 1 mm.

(F, G) Quantification of colony diameter (F) and colony number (G) from Ctrl-T and *Olig2*KO tumor cells, respectively, plated on soft agar.

(H) Tumor cells from Ctrl-T and *Olig2*KO mice were cultured in 1% FBS for 48 hr and stained with anti-GFAP and anti-PDGFR $\alpha$  as indicated. Scale bar, 50  $\mu$ m.

Data are presented as means  $\pm$  SEM from three independent experiments in B, D, F and G. The cross-lines in F represent means  $\pm$  SEM (\*\*  $p < 0.01$ ; \*\*\*  $p < 0.001$ ; Student's  $t$  test). See also Figure S4.



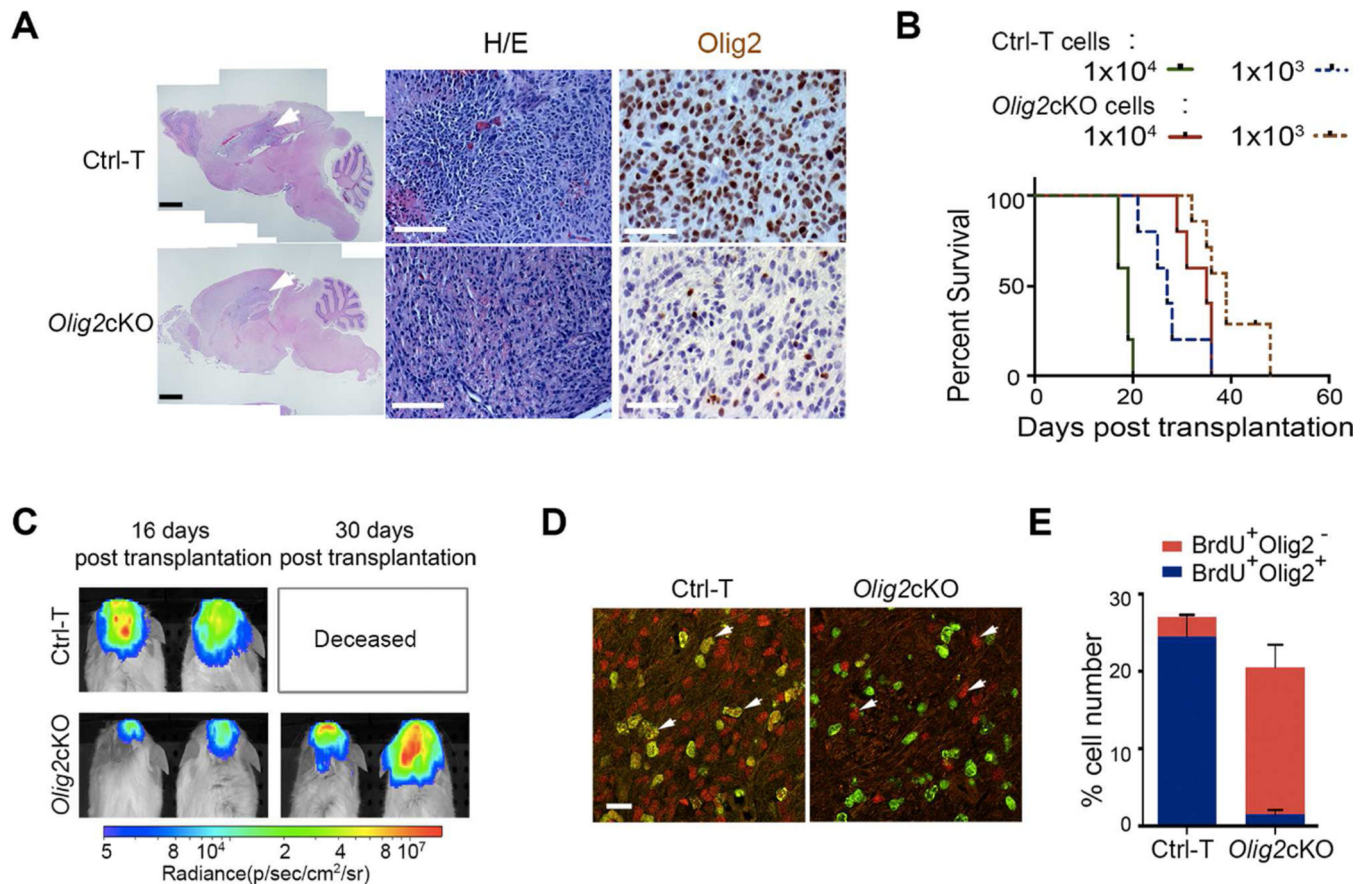


**Figure 5. *Olig2cKO* tumor cells retain tumorigenic capacity**

(A) Tumor cells ( $1 \times 10^4$ ) isolated from Ctrl-T and *Olig2cKO* tumor lesions were intracranially engrafted into the striatum of NSG mice. The tumor tissues were stained with H&E and Olig2 as indicated. Arrows indicate tumor tissues. Scale bars in left, middle and right panels; 1 mm, 100  $\mu$ m and 50  $\mu$ m, respectively.

(B) Kaplan-Meier survival analysis of NSG mice transplanted with  $1 \times 10^4$  Ctrl-T or *Olig2cKO* tumor cells or  $1 \times 10^3$  Ctrl-T or *Olig2cKO* tumor cells ( $p < 0.01$  with the log-rank test between control and *Olig2cKO* group;  $n = 5$  for each group).

(C) Representative in vivo bioluminescence imaging of the NSG mice engrafted with  $1 \times 10^4$  Ctrl-T or *Olig2cKO* tumor cells carrying the Rosa-tmLuciferase reporter at dpi 16 and dpi 30.

(D) Tumor lesions after transplantation of Ctrl-T or *Olig2cKO* tumor cells were immunostained with Olig2 (red) and BrdU (green) after 2-hr pulse-labeling. Arrows indicate Olig2<sup>+</sup> cells. Scale bar, 20  $\mu$ m.

(E) Percentage of BrdU<sup>+</sup> cells among Olig2<sup>+</sup> or Olig2<sup>-</sup> cells in Ctrl-T and *Olig2cKO* orthotopic tumors. Data represent the means  $\pm$  SEM from three mice per group.



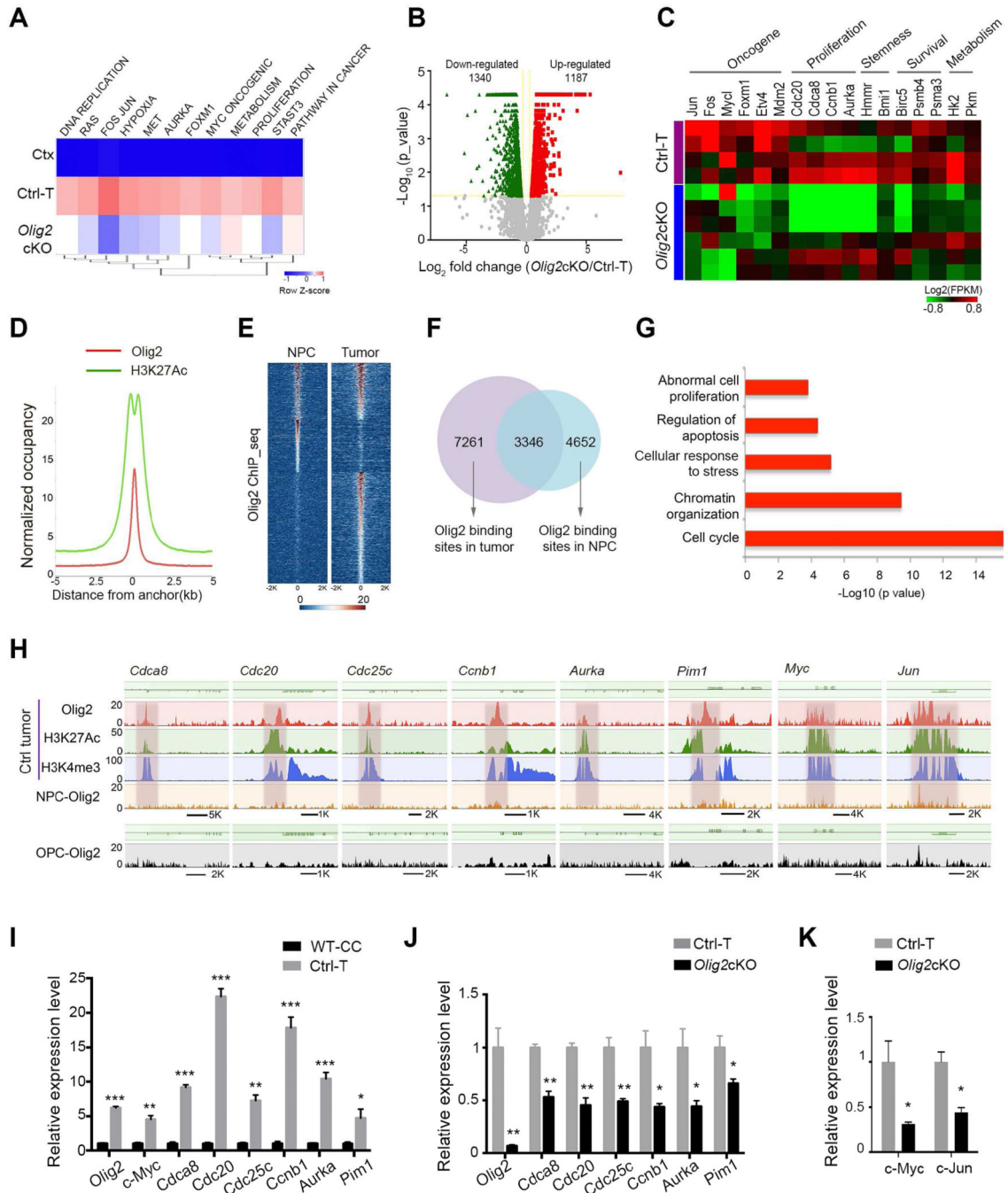


**Figure 6. Olig2 targets the enhancers of cell cycle regulators and oncogenes to regulate cell growth**

(A) Heatmap showing the patterns of pathway activity among normal cortices (n=3), Ctrl-T tumors (n=4) and *Olig2*cKO tumors (n=6) based on the MSigDB database. Expression signature scores are the means and clustered with linkage hierarchical clustering.

(B) Volcano plot of transcriptome expression profiles between the Ctrl-T tumors and *Olig2*cKO tumors. Red and green dots represent genes significantly up-regulated and down-regulated in *Olig2*cKO tumors ( $p < 0.05$ ), respectively.

(C) Heatmap of the genes differentially expressed and associated with tumorigenesis between Ctrl-T tumors (n = 4) and *Olig2*KO tumors (n = 6).

(D) Anchor plot of *Olig2* and H3K27ac ChIP-seq peaks.

(E) Heatmap for signal intensity of *Olig2*-targeted gene loci in Ctrl-T tumors and NPCs.

(F) Venn diagram for *Olig2*-targeted genes detected by ChIP-seq in tumor tissues and NPCs.

(G) GO analysis of biological processes corresponding to *Olig2*-targeted genes in tumor tissues. (H) *Olig2* and histone binding profiles on indicated gene loci in tumor tissues. *Olig2* targeting in NPCs and OPCs is shown in the bottom panels.

(I) qRT-PCR analysis of candidate gene expression in the wild-type corpus callosum (WT-CC) at 8-week old and Ctrl-T tumor tissues at dpi 20.

(J) qRT-PCR analysis of gene expression in Ctrl-T and *Olig2*KO tumor tissue.

(K) qRT-PCR quantification of c-Myc and c-Jun expression in an early stage (dpi 10) Ctrl-T and *Olig2*KO tumors.

Data are presented as the means  $\pm$  SEM from three animals per group in I, J, K (\*  $p < 0.05$ ; \*\*  $p < 0.01$ ; \*\*\*  $p < 0.001$ ; Student's *t* test).

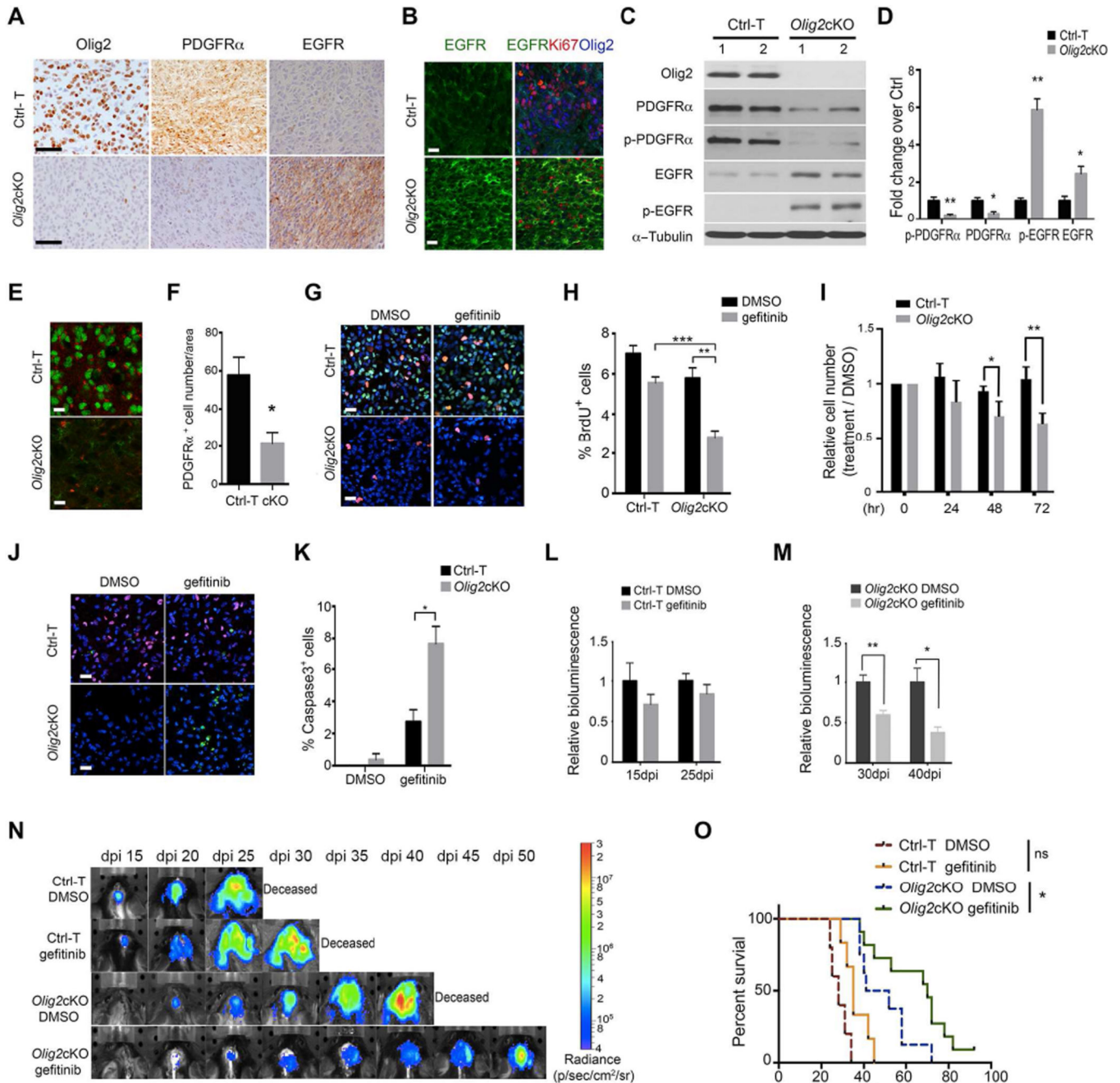


**Figure 7. *Olig2* deletion leads to a tumor phenotype shift from proneural to classical expression pattern**

(A) Scatter plot of RNA-seq data from Ctrl-T and *Olig2*cKO tumors. Examples of significantly ( $p < 0.05$ ) up-regulated and down-regulated genes in *Olig2*cKO as compared to Ctrl-T are represented by red and blue dots, respectively.

(B) ToppCluster analysis shows associated biological processes of genes enriched in Ctrl-T and *Olig2*cKO tumors.

(C) Heatmap indicating expression levels of the “signature” genes in PN and CL GBMs (Verhaak et al., 2010) that are substantially altered in *Olig2*KO tumors as compared to Ctrl-T tumors.

(D) Heatmap of the Ctrl-T-enriched genes and *Olig2*KO-enriched genes in four subtypes of human GBM taken from TCGA unified CORE datasets.

(E) GSEA enrichment plots showing the comparison of gene expression profiles in Ctrl-T and *Olig2*KO tumors with the TCGA signature gene sets in PN, CL, mesenchymal (MES) or neural (NL) GBMs as indicated. NES: normalized enrichment score; p value, represents the statistical significance of the enrichment score; FDR: false discovery rate.

(F) qRT-PCR analysis of expression of representative PN, CL, MES, and NL signature genes between Ctrl-T and *Olig2*KO tumors.

(G) Visualization of *Olig2* binding profiles on the enhancers (marked by H3K27ac) of representative CL signature genes, *Egfr*, *Tbx2*, and *Gli2* in Ctrl-T and *Olig2*KO tumors.

(H) Tumor cells from three different Ctrl-T mice were infected with lentivirus for expression of an shRNA targeting *Olig2* or with an shRNA non-target (NT) control for 4 days. The expression of a set of PN and CL genes was analyzed by qRT-PCR.

(I) Graph of the relative OLIG2 or EGFR expression (Z-score) in PN and CL subtypes of GBMs from the core TCGA samples using the unified scaled data (\*\*\*  $p < 0.001$ ; Student's  $t$  test).

(J) Graph of the relative OLIG2 and EGFR expression in PN or CL subtypes of core TCGA GBMs, respectively.

(K) Primary human GBM clonal cells TS543 were transduced with lentiviral non-target or OLIG2 shRNA vectors carrying a GFP reporter for 72 hr and were pulse-labeled with BrdU for 1 hr. Representative images of the cells immunostained with anti-BrdU and OLIG2 are shown. Arrows: transduced cells. Scale bar, 10  $\mu$ m.

(L) Percentage of BrdU<sup>+</sup> cells transduced with non-target (NT) control shRNA and OLIG2 shRNA in TS543 (left) and TS667 (right).

(M) Primary human proneural GBM clonal cells TS543 (left) and TS667 (right) were infected with lentivirus for non-target (NT) control or OLIG2 shRNA for 84 hr. Expression of a set of proneural and classical tumor associated genes were analyzed by qRT-PCR. Data are presented as the means  $\pm$  SEM from three independent experiments in F, H, L, and M. The cross-lines in I and J represent means  $\pm$  SEM (\*  $p < 0.05$ ; \*\*  $p < 0.01$ ; \*\*\*  $p < 0.001$ ; Student's  $t$  test). See also Figure S5.



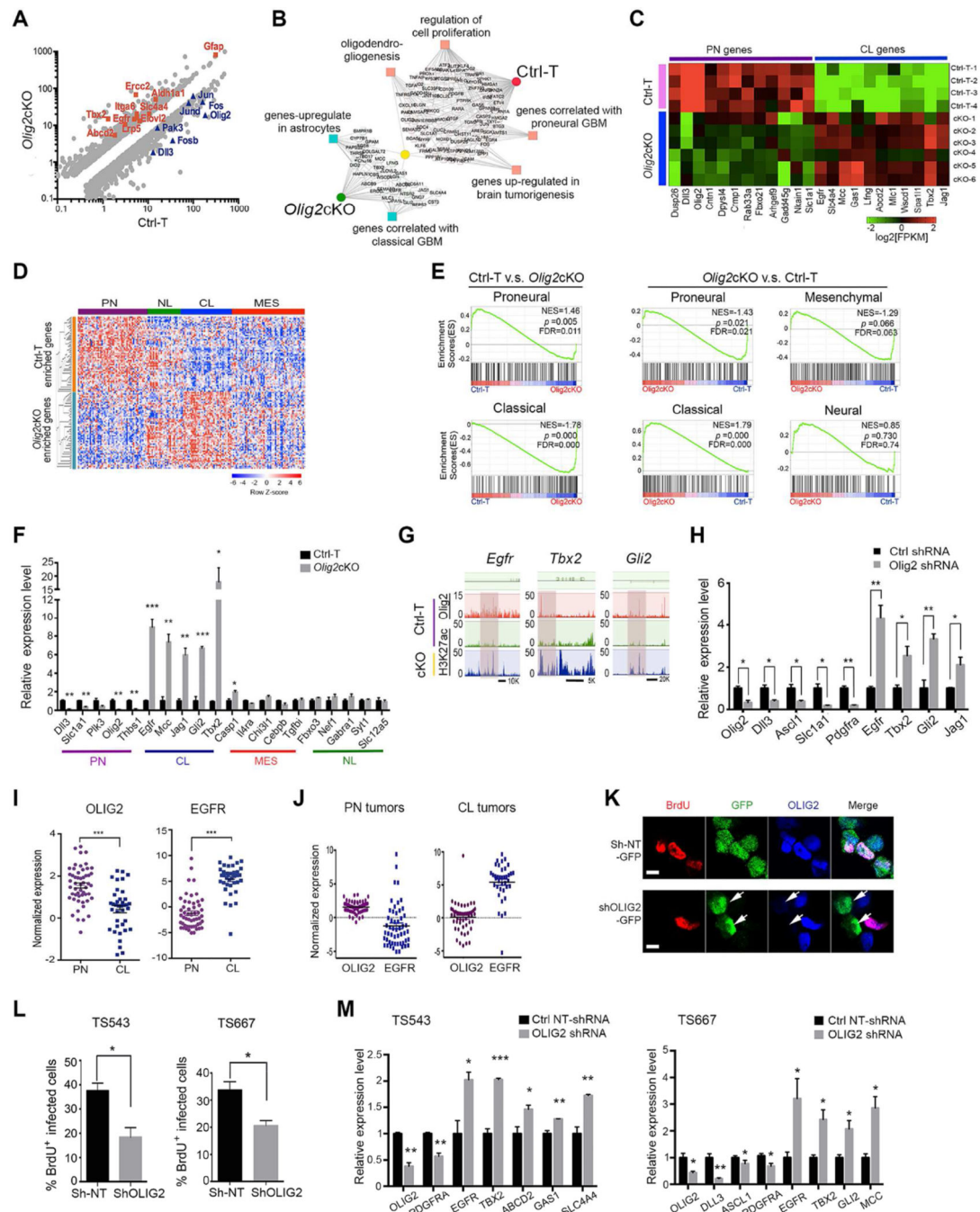


**Figure 8. Targeting EGFR signaling suppresses tumor cell proliferation in *Olig2cKO* mice**  
 (A) Representative immunostaining images of Olig2, PDGFR $\alpha$ , and EGFR in Ctrl-T and *Olig2cKO* tumors. Scale bar, 50  $\mu$ m.  
 (B) Representative immunostaining images for EGFR, Ki67, and Olig2 in Ctrl-T and *Olig2cKO* tumors. Scale bar, 20  $\mu$ m.  
 (C) Representative western blots show expression of PDGFR $\alpha$ , p-PDGFR $\alpha$ , EGFR, p-EGFR in Ctrl-T and *Olig2cKO* tumors.  $\alpha$ -Tubulin as a loading control.

- (D) Quantification of relative expression of PDGFR $\alpha$ , p-PDGFR $\alpha$ , EGFR, and p-EGFR in *Olig2* cKO and Ctrl-T tumors.
- (E) Representative images showing the expression of PDGFR $\alpha$  (red) and Olig2 (green) in Ctrl-T and *Olig2* cKO tumors. Scale bar, 10  $\mu$ m.
- (F) The quantification of PDGFR $\alpha$ <sup>+</sup> cells in Ctrl-T and *Olig2* cKO tumors per unit area (0.04 mm<sup>2</sup>).
- (G) Representative images of BrdU (red) immunostaining of Ctrl-T and *Olig2* cKO tumor cells treated with gefitinib or vehicle (DMSO); Olig2 and DAPI staining was shown in green and blue, respectively. Scale bar, 30  $\mu$ m.
- (H) Percentages of BrdU<sup>+</sup> cells in Ctrl-T and *Olig2* cKO tumor cells treated with gefitinib or DMSO. Data represent the means  $\pm$  SEM from three independent experiments (\*\*  $p < 0.01$ ; \*\*\*  $p < 0.001$ ; ANOVA with Newman–Keuls multiple comparison test).
- (I) Quantification of cells using the CellTiter Glo viability assay from Ctrl-T and *Olig2* cKO tumor cells at indicated times after treatment. Plotted are cell numbers in gefitinib-treated samples divided by cell numbers from DMSO-treated samples.
- (J) Cleaved Caspase 3 staining (green) in Ctrl-T and *Olig2* cKO tumor cells after DMSO or gefitinib treatment; Olig2 staining shown in red; DAPI in blue. Scale bar, 30  $\mu$ m.
- (K) Percentage of cleaved Caspase 3<sup>+</sup> cells in Ctrl-T and *Olig2* cKO tumor cells treated with gefitinib or DMSO.
- (L, M) Relative bioluminescence signals in (L) Ctrl-T mice at dpi 15 and dpi 25 and (M) *Olig2* cKO mice at dpi 30 and dpi 40 treated with DMSO (black) or gefitinib (gray) delivered by osmotic minipumps (n = 6 mice for each group).
- (N) Representative in vivo bioluminescence images of Ctrl-T and *Olig2* cKO mice treated with DMSO or gefitinib at indicated time-points post tumor induction.
- (O) Kaplan-Meier survival analysis of Ctrl-T mice treated with DMSO (brown) or gefitinib (orange), and *Olig2* cKO mice treated with DMSO (blue) or gefitinib (green) delivered by osmotic minipumps.  $p < 0.05$  with the log-rank test between DMSO or gefitinib treated *Olig2* cKO mice. n = 5 mice for each group.
- Data are presented as means  $\pm$  SEM from at least three independent tumor tissue samples per group in D, F, I, K–M (\*  $p < 0.05$ ; \*\*  $p < 0.01$ ; Student's *t* test). See also Figure S6.